

# AUTONOMOUS ORBIT NAVIGATION OF INTERPLANETARY SPACECRAFT

Jo Ryeong Yim,\* John L. Crassidis<sup>†</sup> and John L. Junkins<sup>‡</sup>

*Department of Aerospace Engineering*

Texas A&M University

College Station, TX 77843-3141

## Abstract

In this paper, autonomous orbit navigation of spacecraft for deep space missions is implemented completely independent of a ground tracking system. In order to achieve this aim, the Doppler measurement due to the relative motion from a spacecraft to the Sun is used. Other measurements are the directional data from the spacecraft to the Sun measured from a Sun sensor, and directional data from the spacecraft to the Earth measured from an Earth sensor. The observability of the system with the available measurements is investigated using a linearized observability analysis. Autonomous orbit navigation is obtained by extended Kalman filtering. Results using the Doppler measurement and Sun sensor indicate that autonomous navigation can be accomplished within an accuracy of  $5km$  in position. Adding directional data with respect to the Earth considerably improves the estimate accuracy to within  $3km$ .

## Introduction

In general, orbit determination of a spacecraft involves measurements of range and range rate based on ground tracking or (as a newer technique) signals from GPS receivers.<sup>1</sup> However, ground tracking may incur extensive costs to a spacecraft mission, and GPS is not suitable for deep space missions. Therefore, estimating the orbit without aid from the Earth is needed. The concept of autonomous orbit determination for Earth-orbiting spacecraft without ground tracking or GPS was first proposed and analyzed in Ref. [2]. A batch estimator was designed in Ref. [3] based upon nonlinear least squares to autonomously determine the orbits of two spacecraft from measurements of the relative position vector from one spacecraft to the

other. The estimator in Ref. [3] uses a time series of the inertially-referenced relative position vectors and orbital dynamic models. This concept can be used for absolute orbit determination of formation flying spacecraft. Recently, the idea of autonomous navigation of a spacecraft using celestial objects has been presented using an extended Kalman filter.<sup>4</sup> The measurements used in the simulations are the line of sight directions to the celestial objects from high-accuracy attitude sensors and one-way Doppler measurements from ground stations. Guo<sup>5</sup> has proposed a complete self-contained autonomous navigation system for deep space missions using two types of on-board observation data. The first is a directional data of the spacecraft relative to the Sun, and the second is the optical Doppler shift due to the motion of the spacecraft relative to the Sun.

In general, the light of the Sun can be imaged with a spectrograph or a spectrometer. Due to the relative motion between a light source and a moving object, the spectral lines of light are shifted from the original positions corresponding to their wavelengths, which is called the Doppler shift. Since the shifted amount depends on the relative velocity, a radial velocity can be calculated. The Doppler shift from sunlight can be measured using instruments such as a Doppler compensator and a resonance-scattering spectrometer.<sup>6</sup> According to [6], the Doppler compensator gives an accuracy of  $1 - 10m/sec$  and the resonance-scattering spectrometer has an accuracy of less than  $1cm/s$ . The resonance-scattering spectrometer instrument uses a selected single spectral line, not all spectral lines. When the light comes to the instrument, it passes through a filter, polarizer, and electro-optic modulator. The polarized light shows only one or two shifted components due to a magnetic field in the vapor cell. From these shifted lines, the radial velocity can be measured.

At this point of time, there are several space-based observatories that observe the sun, such as Global Geospace Science (mission operations, Interplan-

\*Graduate Student of Aerospace Engineering.

<sup>†</sup>Assistant Professor of Aerospace Engineering. Senior Member AIAA.

<sup>‡</sup>George J. Eppright Chair Professor of Aerospace Engineering. Fellow AIAA.

Copyright © 2000 by the American Institute of Aeronautics and Astronautics, Inc. All rights reserved.

etary Physics Laboratory WIND, Polar Plasma Laboratory POLAR), SERTS (Solar Extreme-ultraviolet Rocket Telescope and Spectrograph), and SOHO (The Solar and Heliospheric Observatory) (<http://www.lmsal.com/solarsites.html>). Among them, SOHO is a space-based observatory for the helioseismology, which needs to be able to measure the individual oscillation modes that have amplitudes of less than about  $0.1m/s$ . Therefore, a need exists for an instrument that can measure to within an accuracy of less than  $1cm/s$  (<http://soi.stanford.edu/results/heliowhat.html>). This coincides with our need for an instrument to measure a radial velocity measurement.

The work by Guo<sup>5</sup> is extended in this paper by incorporating dynamical models for orbit navigation using a Kalman filter. In order to achieve this aim, it is assumed that the Doppler measurement due to the relative motion from a spacecraft to the Sun is used. Other measurements used in the Kalman filter are the directional data from the given spacecraft to the Sun measured from a Sun sensor, and directional data from the spacecraft to the Earth measured from an Earth sensor.

First, we introduce the equations of motion for an orbiting spacecraft. Next, a summary of the observations equations is given, which uses both velocity measurements and line of sight information. Then, the extended Kalman filter is reviewed. Next, an analysis of the observability of the system using different sensor configurations is shown. Finally, simulation results and discussions are given.

## Equations of Motion

In this paper, the orbit of an interplanetary spacecraft is considered to be estimated. The heliocentric coordinate system (Figure 1) is used in which the origin is the center of the Sun, the fundamental plane is the plane of the ecliptic, the  $x$ -axis directs to the Vernal equinox, the  $y$ -axis is perpendicular to the  $x$ -axis in the fundamental plane, and the  $z$ -axis points out perpendicularly with respect to the fundamental plane at the origin following the right-hand rule.<sup>7</sup> In Figure 1,  $\epsilon$  is the obliquity of ecliptic,  $\beta$  is the celestial latitude and  $\lambda$  is the celestial longitude of an object.

In this initial work, a non-rotating Sun is assumed. The dynamical model equation for a spacecraft moving under the influence of the Sun's gravity is

$$\dot{\mathbf{r}} = \mathbf{v} \quad (1a)$$

$$\dot{\mathbf{v}} = -\frac{\mu_s}{r^3} \mathbf{r} \quad (1b)$$

where the vectors  $\mathbf{r}$  and  $\mathbf{v}$  denote the inertial position and velocity of a spacecraft,  $r = \sqrt{x^2 + y^2 + z^2}$  and  $\mu_s$  is the gravitational mass constant of Sun. It is assumed that there is no external disturbing force for

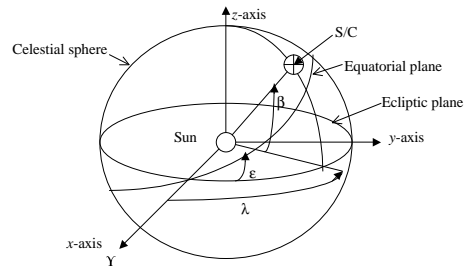


Fig. 1 Heliocentric coordinate system.

the system except the gravitational force between the Sun and an interplanetary spacecraft.

As mentioned previously, there are two kinds of measurements in the filter: a radial velocity and a line of sight vector. Attitude knowledge for an interplanetary spacecraft is assumed to be known; attitude estimation is not considered in this paper. First, a radial velocity  $\dot{r} = v$  can be measured from a Doppler shift due to the relative motion between the Sun and a spacecraft with spectrometer as mentioned in previous section. For simulation purposes, the radial velocity can be modeled by the following equation:

$$\dot{r} \equiv v_r = \frac{\mathbf{r} \cdot \dot{\mathbf{r}}}{r} = \frac{\mathbf{r} \cdot \mathbf{v}}{r} \quad (2)$$

Second, we assume that a measurement of line of sight is available using an optical instrument, so that  $\mathbf{r} = r\hat{\mathbf{l}}$ . In a real system, this measurement should be observed from the given spacecraft to the Sun but here, the line of sight measurement is in the reference frame, since we only deal with the absolute position and velocity with respect to the inertial reference frame. We assume that the line of sight vector is formed using spherical coordinate measurements, so that

$$\hat{\mathbf{l}} = \cos(\Theta) \cos(\Phi) \hat{\mathbf{n}}_1 + \cos(\Theta) \sin(\Phi) \hat{\mathbf{n}}_2 + \sin(\Theta) \hat{\mathbf{n}}_3 \quad (3)$$

where  $\Phi$  (azimuth angle) and  $\Theta$  (elevation angle) are considered to be measured. Figure 2 shows the graphical concept of the orbit of an interplanetary spacecraft, the radial velocity measurement  $v_r$ , and the line of sight vector  $\hat{\mathbf{l}}$ . From this line of sight vector, two angles  $\Phi$  and  $\Theta$  can be modeled as follows:

$$\Phi = \tan^{-1} \left( \frac{y}{x} \right) \quad (4a)$$

$$\Theta = \sin^{-1} \left( \frac{z}{r} \right) \quad (4b)$$

To improve the estimation accuracy, an additional measurement is introduced, which is a line of sight vector  $\hat{\mathbf{l}}_{se}$  measured from a given spacecraft to the Earth. The description of this measurement is shown in Figure 3 as well as the Doppler measurement and the

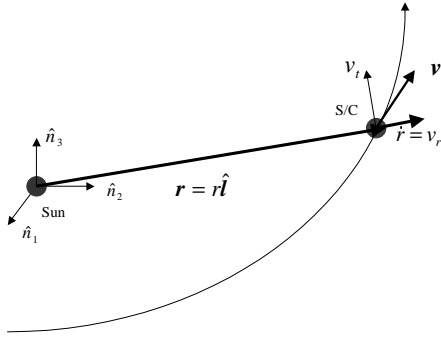


Fig. 2 Diagram of an orbit and Sun measurements.

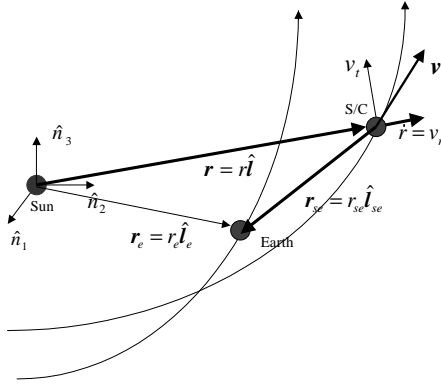


Fig. 3 Diagram of an orbit and Earth measurements.

line of sight measurement with respect to the Sun. An orbit of the Earth can be obtained by the same forcing equation as Eq. (1) replacing  $\mathbf{r}$  and  $\mathbf{v}$  by  $\mathbf{r}_e$  and  $\mathbf{v}_e$  for position and velocity vector, and then  $r_e$  is  $\sqrt{x_e^2 + y_e^2 + z_e^2}$ . The line of sight vector between the interplanetary spacecraft and the Earth can be written in the same manner as the line of sight vector between the Sun and a spacecraft as

$$\hat{\mathbf{l}}_{se} = \cos(\Theta_{se}) \cos(\Phi_{se}) \hat{\mathbf{n}}_1 + \cos(\Theta_{se}) \sin(\Phi_{se}) \hat{\mathbf{n}}_2 + \sin(\Theta_{se}) \hat{\mathbf{n}}_3 \quad (5)$$

Now, the measurement from this line of sight vector can be expressed as

$$\Phi_{se} = \tan^{-1} \left( \frac{y_e - y}{x_e - x} \right) \quad (6a)$$

$$\Theta_{se} = \sin^{-1} \left( \frac{z_e - z}{r_e - r} \right) \quad (6b)$$

where  $\Phi_{se}$  is an azimuth angle and  $\Theta_{se}$  is an elevation angle of the Earth, when they are viewed from an interplanetary spacecraft to the Earth in the inertial reference frame.

## Extended Kalman Filter

An extended Kalman filter is used for position and velocity estimation. The standard orbit model in Eq. (1) can be written in the general state equation form which can be used for the propagation of the states in the filter as

$$\dot{\mathbf{x}} = \mathbf{f}(\mathbf{x}, t) + \mathbf{w}(t) \quad (7)$$

where  $\mathbf{x} = [\mathbf{r}^T \mathbf{v}^T]^T$  and  $\mathbf{w}$  is a process noise term. In general, the discrete measurement equation can be expressed for the filter as

$$\tilde{\mathbf{y}}_k = \mathbf{h}_k(\mathbf{x}_k, t_k) + \mathbf{v}_k \quad (8)$$

where  $\tilde{\mathbf{y}}$  is a measurement vector and  $\mathbf{v}$  is a measurement noise which is assumed to be a white Gaussian noise process. In order to use a recursive filter, we need to express the state and measurement equation in the linearized form. When the first order expansion is used for above nonlinear equation, it can be rewritten to be

$$\delta \dot{\mathbf{x}} = F \delta \mathbf{x} + G \mathbf{w} \quad (9a)$$

$$\delta \tilde{\mathbf{y}} = H \delta \mathbf{x} + \mathbf{v} \quad (9b)$$

where

$$F \equiv \frac{\partial \mathbf{f}}{\partial \mathbf{x}} \quad (10a)$$

$$G \equiv \frac{\partial \mathbf{f}}{\partial \mathbf{w}} \quad (10b)$$

$$H \equiv \frac{\partial \mathbf{h}}{\partial \mathbf{x}} \quad (10c)$$

$$E\{\mathbf{w} \mathbf{w}^T\} = Q \quad (10d)$$

$$E\{\mathbf{v}_k \mathbf{v}_k^T\} = R \quad (10e)$$

where  $\mathbf{w}$  and  $\mathbf{v}$  are assumed to be uncorrelated,  $Q$  and  $R$  are process noise weight matrix and measurement noise weight matrix with zero mean, respectively. Since the state equation is a standard orbit model, the Jacobian matrix of the state equation is given by

$$\frac{\partial \mathbf{f}}{\partial \mathbf{x}} = F = \begin{bmatrix} 0_{3 \times 3} & I_{3 \times 3} \\ G_{3 \times 3} & 0_{3 \times 3} \end{bmatrix} \quad (11)$$

and  $G$  is a gravity gradient matrix which can be written by

$$G = \begin{bmatrix} -\frac{\mu_s}{r^3} + \frac{3\mu_s x^2}{r^5} & \frac{3\mu_s xy}{r^5} & \frac{3\mu_s xz}{r^5} \\ \frac{3\mu_s xy}{r^5} & -\frac{\mu_s}{r^3} + \frac{3\mu_s y^2}{r^5} & \frac{3\mu_s yz}{r^5} \\ \frac{3\mu_s xz}{r^5} & \frac{3\mu_s yz}{r^5} & -\frac{\mu_s}{r^3} + \frac{3\mu_s z^2}{r^5} \end{bmatrix} \quad (12)$$

In order to obtain the partial of the measurement equation, Eq. (2) can be reformulated as

$$r \cdot \dot{r} = \mathbf{r} \cdot \mathbf{v} \quad (13)$$

From the above expression, the partial of a radial velocity with respect to each state is given by

$$\frac{\partial \dot{r}}{\partial \mathbf{x}} = \frac{1}{r} \left[ \frac{\partial \mathbf{r}}{\partial \mathbf{x}} \dot{\mathbf{r}} + \mathbf{r} \frac{\partial \dot{\mathbf{r}}}{\partial \mathbf{x}} - \frac{\partial r}{\partial \mathbf{x}} \dot{r} \right] \quad (14)$$

Let  $X$  be  $y/x$  and  $Y$  be  $z/r$ . Then the line of sight measurements can be expressed as

$$\frac{\partial \Phi}{\partial \mathbf{x}} = \frac{1}{1+X^2} \frac{\partial X}{\partial \mathbf{x}} \quad (15)$$

$$\frac{\partial \Theta}{\partial \mathbf{x}} = \frac{1}{\sqrt{1-Y^2}} \frac{\partial Y}{\partial \mathbf{x}} \quad (16)$$

Now, the above partials of measurement equations can be used in the filter. In the extended Kalman filter, the state can be updated when new measurements are available using the equation:<sup>8</sup>

$$\hat{\mathbf{x}}_k^+ = \hat{\mathbf{x}}_k^- + K_k [\tilde{\mathbf{y}}_k - \mathbf{h}_k(\hat{\mathbf{x}}_k^-)] \quad (17)$$

where the superscripts  $+$  and  $-$  denote the estimate at the measurement update time and propagation time, respectively, and  $K$  is a gain at the measurement time update given by

$$K_k = P_k^- H_k^T [H_k P_k^- H_k^T + R]^{-1} \quad (18)$$

and here  $P_k^+$  is an updated error covariance matrix

$$P_k^+ = [I - K_k H_k] P_k^- \quad (19)$$

and  $P_k^-$  is an error covariance matrix before the update which comes from the integration of the following equation

$$\dot{P} = AP + PA^T + GQG^T \quad (20)$$

Also, the state propagation is given by the following equation

$$\dot{\hat{\mathbf{x}}} = \mathbf{f}(\hat{\mathbf{x}}, t) \quad (21)$$

Equations (17) to (21) represent the extended Kalman filter that is used to estimate the orbital position and velocity.

## Observability

The performance of a filter can be checked by investigating the observability of the given system with various available measurements. The controllability and the observability were analyzed by Ref. [9] for nonlinear systems. Observability of a nonlinear system can be characterized from a differential geometric point of view. Consider the following system  $\Sigma$ :

$$\Sigma \begin{cases} \dot{\mathbf{x}} = \mathbf{f}(\mathbf{x}) \\ \mathbf{y} = \mathbf{g}(\mathbf{x}) \end{cases} \quad (22)$$

where  $\mathbf{x} \in N$ , a  $C^\infty$  connected manifold of dimension  $n$ ,  $\mathbf{y} \in \mathfrak{R}^m$  and  $\mathbf{f}$  and  $\mathbf{g}$  are  $C^\infty$  functions. A pair of points  $\mathbf{x}_0$  and  $\mathbf{x}_1$  are indistinguishable if  $(\Sigma, \mathbf{x}_0)$  and

$(\Sigma, \mathbf{x}_1)$  realize the same input-output map. Indistinguishability  $I$  is an equivalence relation on  $N$ . The system  $\Sigma$  is locally weakly observable at  $\mathbf{x}_0$  if there exists an open neighborhood  $U$  of  $\mathbf{x}_0$  such that for every neighborhood  $V$  of  $\mathbf{x}_0$  contained in  $U$ ,  $I_V(\mathbf{x}_0) = \{\mathbf{x}_0\}$  and is locally weakly observable if it is so at every  $x \in N$ .<sup>9</sup> Local weak observability can be checked by an algebraic test using linear operators on  $C^\infty(N)$  by Lie differentiation:

$$L_f \mathbf{g}(\mathbf{x}) = \frac{\partial \mathbf{g}}{\partial \mathbf{x}} \mathbf{f}(\mathbf{x}) \quad (23)$$

If  $\mathbf{g}$  is differentiated  $k$  times along  $\mathbf{f}$ , the notation  $L_f^k \mathbf{g}(\mathbf{x})$  is used, defined as

$$L_f^k \mathbf{g}(\mathbf{x}) = \frac{\partial (L_f^{k-1} \mathbf{g})}{\partial \mathbf{x}} \mathbf{f}(\mathbf{x}) \quad (24)$$

with  $L_f^0 \mathbf{g}(\mathbf{x}) = \mathbf{g}(\mathbf{x})$ . Also, for simplicity the following partial derivative is defined:

$$dg = \frac{\partial \mathbf{g}}{\partial \mathbf{x}} \quad (25)$$

It is straightforward to show that the orbital and observation equations used in this paper are closed with respect to Lie differentiation. Local observability can be checked by forming the following matrix:

$$O = \begin{bmatrix} dg(\mathbf{x}) \\ dL_f \mathbf{g}(\mathbf{x}) \\ \vdots \\ dL_f^{n-2} \mathbf{g}(\mathbf{x}) \\ dL_f^{n-1} \mathbf{g}(\mathbf{x}) \end{bmatrix} \quad (26)$$

If  $\Sigma$  satisfies the observability rank condition (i.e.,  $O$  has rank  $n$ ) at  $\mathbf{x}_0$ , then  $\Sigma$  is locally weakly observable at  $\mathbf{x}_0$ . In this analysis the matrix  $O$  is formed at one instant of time. Global observability is difficult to prove, although a version of the extended Kalman filter in a special coordinate system has been shown to asymptotically converge.<sup>10</sup> In this paper the observability matrix is accumulated over the entire time from the initial time  $t_0$  to the final time  $t_f$  (i.e., the set that contains all  $\mathbf{x}$  in  $t$ ) as a global check. This approach does not guarantee convergence in the extended Kalman filter; however, we have found it useful to quantify the relative observability between various sensor configurations.

Using the observability matrix in Eq. (26), the singular value decomposition is performed as

$$O = \mathbf{U} \Sigma \mathbf{V}^T \quad (27)$$

where  $\Sigma$  is a diagonal matrix of singular values and  $\mathbf{U}$  and  $\mathbf{V}$  are unitary matrices. The singular values give an indication of the rank of the observability matrix. When  $\Sigma$  has rank  $n$ , which is the system order, the

**Table 1** Position and velocity at initial and final time.

	Initial $\mathbf{r}$ and $\mathbf{v}$	Final $\mathbf{r}$ and $\mathbf{v}$
$x$	$1.500 \times 10^8$	$1.4030 \times 10^7$
$y$	$2.814 \times 10^7$	$1.577 \times 10^8$
$z$	$9.444 \times 10^5$	$5.293 \times 10^6$
$\dot{x}$	-4.5653	28.38
$\dot{y}$	29.28	3.045
$\dot{z}$	0.9824	0.1022

**Table 2** Orbital elements used in simulations.

Semimajor axis	$a = 1.5426 \times 10^8 km$
Eccentricity	$e = 0.033$
Inclination	$i = 1.92 \text{ deg}$
Node right ascension	$\Omega = 0 \text{ deg}$
Argument of perigee	$\omega = 297.9 \text{ deg}$
Period	$T = 3.305 \times 10^7 s$

system is fully observable. On the contrary, when  $\Sigma$  has rank less than  $n$ , the overall system is unobservable; however, the magnitude of each singular value gives an indication of the degree of observability. Any state corresponding to a larger singular value is more observable than any state corresponding to a smaller value. From the companion matrix  $\mathbf{V}^T$  of the singular value decomposition, the state corresponding to each singular value can be found. A column of the matrix  $\mathbf{V}^T$  corresponds to each singular value and the numbers in each element in any column represents each state. For example, the column corresponding to the largest singular value means that this column gives the most observable information, and the state corresponding to the largest number in the column of  $\mathbf{V}^T$  is the most observable state. In the same manner, the column corresponding to the smallest singular value gives the least observable information, and the state corresponding to the largest number in the column of  $\mathbf{V}^T$  is the least observable state.

In order to check the observability, an orbit trajectory of an interplanetary spacecraft is chosen similar to the Earth's trajectory. The initial and the final values of the spacecraft position in  $km$  and velocity in  $km/s$  are shown in Table 1. Figure 4 shows the trajectory of the interplanetary spacecraft with the Sun in the center. The orbit elements corresponding to the above initial conditions are shown in Table 2.

Two sensor cases are investigated: the first uses the Doppler measurement and directional data to the Sun as measurements, and the second adds one more measurement of directional data to the Earth. To be fully observable, the observability matrix should have rank 6. It may not be possible to estimate the orbit of a spacecraft using only the radial velocity measurement with respect to the Sun since the rank of the observability matrix has less than 6, i.e. rank 4 in this case.

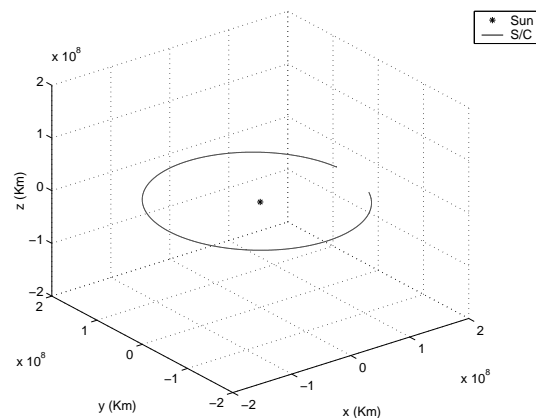


**Fig. 4** Position of an Interplanetary S/C.

Table 3 shows the singular values and the columns of  $\mathbf{V}^T$  for this case. In the first column, two of the singular values are zero up to 16 significant digits. A condition number can be obtained by dividing the largest singular value by the smallest singular value. The condition number for this case is  $1.58255 \times 10^{20}$ . Column 1 of the  $\mathbf{V}^T$  matrix corresponds to the largest singular value. The fourth element in this column has the largest number, which means that the state  $\dot{x}$  is the most observable state for this case. In column 2 the 3rd element has the largest number, and in column 3 the 6th element has the largest number. Using the same insight to other columns, we can find which state is most observable and which state is least observable. In column 6 the fifth element has the largest value, which means that the state  $\dot{y}$  is least observable. As seen from Table 3, we infer the most observable state to the least observable state is in the order of  $\dot{x}$ ,  $z$ ,  $\dot{z}$ ,  $x$ ,  $y$ , and  $\dot{y}$ . Simulation results indicate that the extended Kalman filter does not converge using only velocity measurements, as expected from the observability analysis. Therefore, additional information is required. Sun sensors can provide a directional measurement with respect to the Sun. Additional, Earth sensors provide a line of sight vector to the Earth. Therefore, both sets of information can be added as additional measurements to estimate the complete orbital position and velocity.

Table 4 shows the singular values in decreasing order of their sizes which are obtained from two measurements using velocity and Sun sensor information (Case I), and from velocity, Sun sensor and Earth sensor information (Case II). As shown in Table 4, Case II is clearly more observable than Case I. For Case I, the condition number is approximately  $2.5 \times 10^{10}$ . For Case II, the condition number is decreased up to about  $3.71 \times 10^8$  even though this case has the same largest singular value as Case I. Therefore, we can conclude that adding one more measurement from the

**Table 3 Singular values and the companion matrix  $\mathbf{V}^T$ .**

SV	column 1	column 2	column 3	column 4	column 5	column 6
908	$1.97 \times 10^{-8}$	$1.58 \times 10^{-7}$	$5.31 \times 10^{-9}$	0.938	-0.345	-0.0116
2.41	$-3.68 \times 10^{-7}$	$-5.02 \times 10^{-8}$	$-1.69 \times 10^{-9}$	-0.345	-0.938	-0.03148
$1.76 \times 10^{-9}$	0.443	0.896	0.0301	$-2.13 \times 10^{-7}$	$-1.09 \times 10^{-5}$	0.000322
$2.0 \times 10^{-12}$	-0.896	0.442	0.0149	$3.21 \times 10^{-8}$	-0.00124	0.0369
0	0.0329	-0.0166	$-8.47 \times 10^{-4}$	$-6.75 \times 10^{-7}$	-0.0335	0.999
0	$-3.54 \times 10^{-5}$	0.0336	-0.999	$1.96 \times 10^{-10}$	$9.65 \times 10^{-6}$	-0.000288

**Table 5 Companion matrix  $\mathbf{V}^T$  for two measurement case.**

	column 1	column 2	column 3	column 4	column 5	column 6
$x$	$1.97 \times 10^{-8}$	$1.58 \times 10^{-7}$	$5.31 \times 10^{-9}$	0.938	-0.345	-0.0116
$y$	$-3.96 \times 10^{-7}$	$-1.65 \times 10^{-7}$	$-2.12 \times 10^{-7}$	-0.345	-0.938	-0.0390
$z$	$2.11 \times 10^{-8}$	$5.14 \times 10^{-7}$	$-2.73 \times 10^{-5}$	$2.61 \times 10^{-3}$	0.0406	-0.999
$\dot{x}$	$-3.28 \times 10^{-4}$	-0.0182	0.9998	$-3.11 \times 10^{-9}$	$9.13 \times 10^{-7}$	$-2.73 \times 10^{-5}$
$\dot{y}$	0.236	0.972	0.0178	$-2.38 \times 10^{-7}$	$-1.88 \times 10^{-7}$	$1.25 \times 10^{-8}$
$\dot{z}$	-0.972	0.236	0.00397	$1.02 \times 10^{-7}$	$3.30 \times 10^{-7}$	$6.25 \times 10^{-9}$

**Table 4 Singular values of the observability matrix.**

	Case I	Case II
1	907.754	907.758
2	2.41436	14.0824
3	1.43947	12.0302
4	$2.68233 \times 10^{-5}$	$2.62769 \times 10^{-4}$
5	$5.34681 \times 10^{-6}$	$2.33333 \times 10^{-4}$
6	$3.1682 \times 10^{-8}$	$3.62553 \times 10^{-6}$

Earth sensor makes the given system more observable. For deep space missions, the directional data from a spacecraft to the Earth can be substituted with the directional data of any other planet near the given spacecraft. Table 5 shows the 6 column matrix  $\mathbf{V}^T$  obtained by using two measurements (Case I). For this system, the position vector is weakly observable compared to the velocity vector. From column 1 of  $\mathbf{V}^T$  matrix, we can see that the state  $\dot{z}$  is the most observed state, while from the last column of  $\mathbf{V}^T$ , the state  $z$  is the least observed state. As a whole, using two measurements (radial velocity and a line of sight with respect to the Sun), all states can be well estimated, with the degree from the most observable state to the least observable state in the order of  $\dot{z}$ ,  $\dot{y}$ ,  $\dot{x}$ ,  $x$ ,  $y$ , and  $z$ .

Table 6 shows the 6 column matrix  $\mathbf{V}^T$  obtained by using three measurements (Case II). Adding the Earth sensor measurement make the system much more coupled from an observability sense. For this case, the states can be well observed in the order of  $\dot{z}$ ,  $\dot{y}$ ,  $\dot{x}$ ,  $x$ ,  $z$ , and  $y$ . The state  $y$  is the least observable state. In this case the position vector is the least observable state, which is the same result given in the two measurement case. This analysis indicates that the Kalman filter can be considerably improved by using three measure-

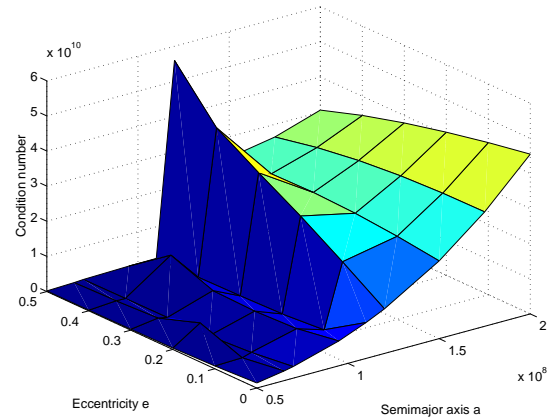


**Fig. 5 Condition number between semimajor axis and eccentricity.**

ments (i.e., the filter should be able to converge better by using all three measurements). This result is shown in the next section.

We now consider the effects of the observability directly on the orbital elements in order to provide more physical meaning. We only show results for the two measurement case (Case I). The condition numbers of the observability matrix are computed for two cases. The first gives the condition number for varying values between the semimajor axis  $a$  and eccentricity  $e$  with constant inclination  $i$  set at 0 degrees. The second gives the condition number for varying values between the semimajor axis  $a$  and inclination  $i$  with constant eccentricity  $e$  set at 0. All other orbit elements are fixed as constants. For both cases, the semimajor axis varies from  $0.5 \times 10^8 km$  to  $2 \times 10^8 km$ . The eccentricity varies from 0 to 0.5 at 0.1 increments, and the

**Table 6 Companion matrix  $V^T$  for three measurement case.**

	column 1	column 2	column 3	column 4	column 5	column 6
$x$	$2.02 \times 10^{-8}$	$1.59 \times 10^{-7}$	$5.62 \times 10^{-9}$	0.938	-0.345	-0.0116
$y$	$-2.75 \times 10^{-6}$	$-8.19 \times 10^{-6}$	$2.58 \times 10^{-5}$	-0.102	-0.309	0.946
$z$	$-1.39 \times 10^{-5}$	$-2.12 \times 10^{-5}$	$-8.77 \times 10^{-6}$	-0.330	-0.886	-0.325
$\dot{x}$	-0.128	-0.342	0.931	$3.11 \times 10^{-6}$	$9.15 \times 10^{-6}$	$-2.54 \times 10^{-5}$
$\dot{y}$	-0.512	-0.781	-0.357	$8.84 \times 10^{-6}$	$2.33 \times 10^{-5}$	$1.01 \times 10^{-5}$
$\dot{z}$	-0.849	0.523	0.0758	$-4.75 \times 10^{-8}$	$6.29 \times 10^{-8}$	$8.25 \times 10^{-9}$

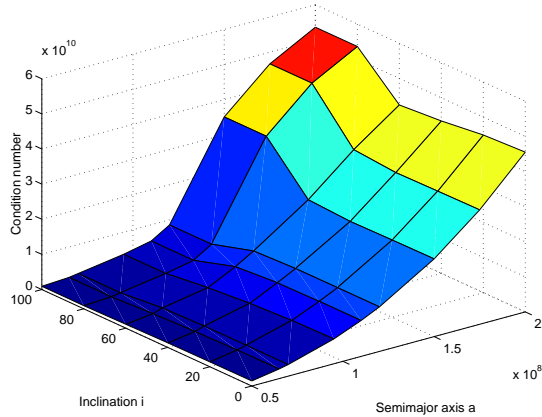


**Fig. 6 Condition number between semimajor axis and inclination.**

inclination varies from 0 deg to 100 deg at 20 deg increments. The results are shown in Figure 5 and Figure 6 for each case, respectively. In Figure 5, the observability decreases as the semimajor axis increases, since the condition number increases as the semimajor axis increases. As a whole, the trend shows that the observability increases as the eccentricity increases except in a few semimajor axis cases.

In Figure 6, the trend shows that the observability increases as the inclination increases up to about 50 deg. When the inclination is greater than 50 deg, the system observability decreases. For this case, the radial velocity measurements at all times are the same since the eccentricity is fixed as 0. However, the angular measurements  $\Phi$  and  $\Theta$  are influenced by a change in the inclination. Figure 6 shows the various inclination changes (and thus changes in  $\Phi$  and  $\Theta$ ) for varying semimajor axis. For every value of the semimajor axis, an inclination of 45 degrees gives the most observable information.

### Simulation Results

The orbital elements for the simulations are given in Table 2. The standard deviation of the measurement error for the radial velocity is assumed to be  $1 \times 10^{-5} km/s$  (i.e.  $1cm/s$ ) according to Ref. [6]. The angle error is assumed to be  $1.745 \times 10^{-6} rad$  following the conventional measurement accuracy for the directional measurement. The process noise matrix  $Q$  in

the Kalman is assumed to be  $O_{6 \times 6}$ , following the traditional approach for orbit determination. There is no process noise term used for the state propagation since we assume that the dynamical model for the state is perfect Keplerian motion. The measurement noise weight matrix  $R$  is

$$R = \begin{bmatrix} 0.00001^2 & 0 & 0 \\ 0 & 0.000001745^2 & 0 \\ 0 & 0 & 0.000001745^2 \end{bmatrix} \quad (28)$$

The initial estimates for the states are 1% off from the true initial state values. This corresponds to a very large error of about  $1.5 \times 10^6 km$  for position in the  $x$ -axis. The initial error covariance  $P_0$  is theoretically an expectation value of  $E\{(\mathbf{x}_0 - \hat{\mathbf{x}}_0)(\mathbf{x}_0 - \hat{\mathbf{x}}_0)^T\}$ . Here,  $\hat{\mathbf{x}}_0$  is the initial estimated state vector. For two measurements case, the initial error covariance adopted is a diagonal matrix given by

$$P_0 = 1.0 \times 10^{14} \begin{bmatrix} 1^2 & 0 & 0 & 0 & 0 & 0 \\ 0 & 1^2 & 0 & 0 & 0 & 0 \\ 0 & 0 & 1^2 & 0 & 0 & 0 \\ 0 & 0 & 0 & a & 0 & 0 \\ 0 & 0 & 0 & 0 & a & 0 \\ 0 & 0 & 0 & 0 & 0 & a \end{bmatrix} \quad (29)$$

where  $a = (1 \times 10^{-7})^2$ . The filter is not sensitive to the initial error covariance if the order of the initial error covariance is greater than  $1.0 \times 10^{10}$  and smaller than  $1.0 \times 10^{20}$ . Using the Doppler measurement and the Sun sensor measurements, the estimation errors for the position and velocity are shown in Figure 7 and Figure 8 with the theoretical  $3\sigma$  outliers computed from the diagonal elements of the covariance matrix. The estimation accuracy is obtained to within about  $5km$  in position and to within  $1 \times 10^{-6} km/sec$  in velocity.

In order to obtain more precise estimates, the line of sight vector to the Earth is added as another measurement. The initial error covariance is given by

$$P_0 = 1.0 \times 10^{18} \begin{bmatrix} 1^2 & 0 & 0 & 0 & 0 & 0 \\ 0 & 1^2 & 0 & 0 & 0 & 0 \\ 0 & 0 & 1^2 & 0 & 0 & 0 \\ 0 & 0 & 0 & a & 0 & 0 \\ 0 & 0 & 0 & 0 & a & 0 \\ 0 & 0 & 0 & 0 & 0 & a \end{bmatrix} \quad (30)$$

where  $a = (1 \times 10^{-7})^2$ . This case works well with the initial error covariance order from  $1.0 \times 10^{18}$  to

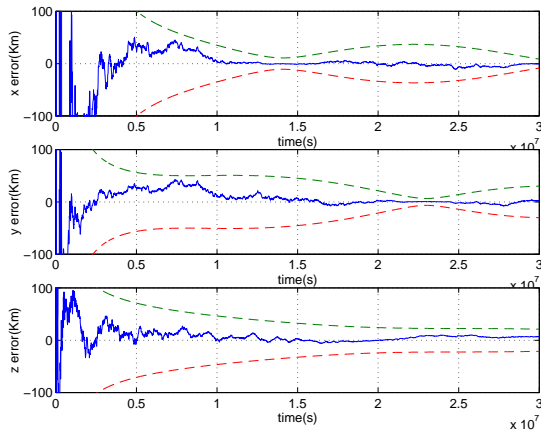


Fig. 7 Position error with  $3\sigma$  outliers for two measurements.

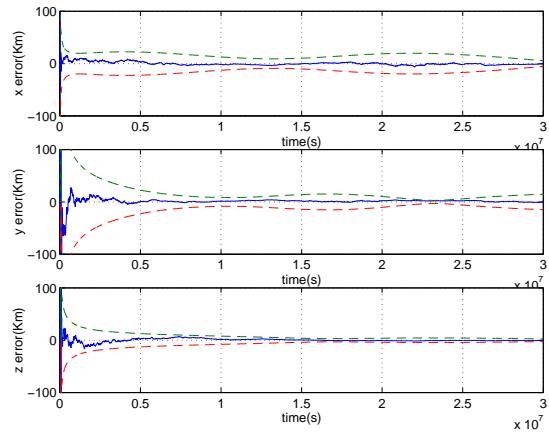


Fig. 9 Position error with  $3\sigma$  outliers for three measurements.

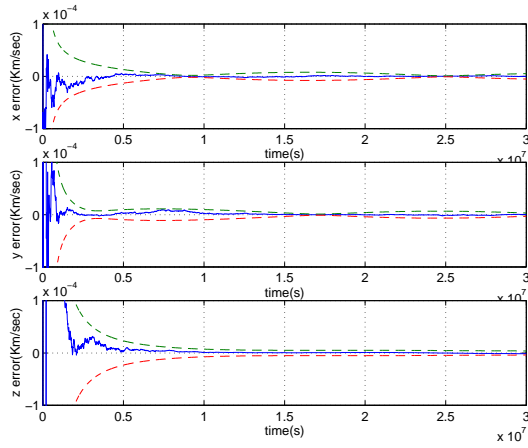


Fig. 8 Velocity error with  $3\sigma$  outliers for two measurements.

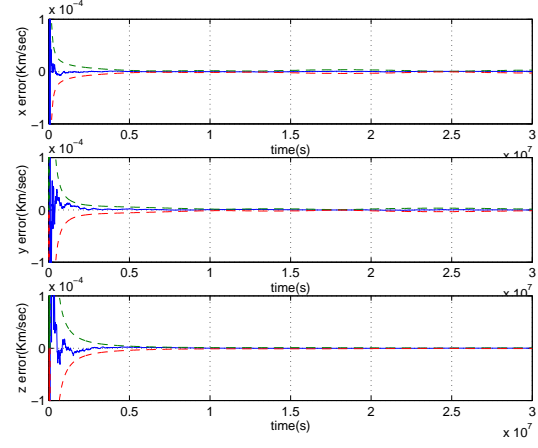


Fig. 10 Velocity error with  $3\sigma$  outliers for three measurements.

Table 7  $3\sigma$  outliers of position and velocity at  $t = t_f$ .

	Case I	Case II
$x$	8.57036	5.39141
$y$	30.1329	14.7696
$z$	21.1996	2.49821
$\dot{x}$	$5.08885 \times 10^{-6}$	$2.85665 \times 10^{-6}$
$\dot{y}$	$3.13851 \times 10^{-6}$	$1.45402 \times 10^{-6}$
$\dot{z}$	$3.92841 \times 10^{-6}$	$7.26774 \times 10^{-7}$

$1.0 \times 10^{20}$ , which is a smaller range than in Case I. The estimation errors for the position and velocity are shown in Figures 9 and 10 with  $3\sigma$  outliers. The estimation accuracy is considerably improved from the previous case to within about  $3km$  in position and  $1 \times 10^{-7}km/sec$  in velocity. In order to compare the filter accuracy, the  $3\sigma$  error outliers at the final time  $t_f$  for both cases are computed and shown in Table 7. From Table 7, the estimation errors are much smaller

by using the Earth sensor as an additional measurement, with the  $z$ -axis showing the largest improvement in accuracy.

## Conclusions

The autonomous orbit navigation problem has been considered using various sensor configurations involving radial velocity from Doppler measurements and line of sight measurements to the Sun and Earth. An observability analysis has been performed for the various sensor configurations in order to quantify the expected performance of the extended Kalman filter. This analysis indicates that using only the radial velocity measurement, it is not possible to estimate all orbital states. Autonomous orbit navigation can be possible by using a radial velocity and a line of sight with respect to the Sun. By adding one more line of sight measurement from an Earth sensor, the estimation accuracy can be considerably improved. Results indicate that the velocity states can be estimated very

well with an accuracy of  $1 \times 10^{-7} km/sec$  ( $0.01 cm/sec$ ), and the position states with an accuracy of less than  $3 km$ . Results from this work clearly show that a fully autonomous orbit navigation system is feasible, assuming a suitable reason for measuring Doppler shift of Sun light is developed and implemented.

## References

<sup>1</sup>Yunck, T. P., "Orbit Determination," *Global Positioning System: Theory and Applications*, edited by B. Parkinson and J. Spilker, Vol. 164 of *Progress in Astronautics and Aeronautics*, chap. 21, American Institute of Aeronautics and Astronautics, Washington, DC, 1996.

<sup>2</sup>Markley, F. L., "Autonomous Navigation Using Landmark and Intersatellite Data," *AIAA/AAS Astrodynamics Conference*, Seattle, WA, Aug. 1984, pp. 1–11, AIAA-84-1987.

<sup>3</sup>Psiaki, M. L., "Autonomous Orbit Determination for Two Spacecraft from Relative Position Measurements," *Journal of Guidance, Control, and Dynamics*, Vol. 22, No. 2, 1999, pp. 305–312.

<sup>4</sup>Folta, D. C., Gramling, C. J., A. C., L., Leung, D. S. P., and Belur, S. V., "Autonomous Navigation Using Celestial Objects," *AAS/AIAA Astrodynamics Conference*, Girdwood, AK, Aug. 1999, AAS-99-439.

<sup>5</sup>Guo, Y., "Self-contained Autonomous Navigation System for Deep Space Mission," *AAS/AIAA Space Flight Mechanics Meeting*, Breckenridge, CO, Feb. 1999, AAS-99-177.

<sup>6</sup>Stix, M., *The Sun*, Springer-Verlag, Berlin Heidelberg, 1989.

<sup>7</sup>Escobal, P. R., *Methods of Orbit Determination*, Robert E. Krieger Publishing Co., Inc., Huntington, NY, 1975.

<sup>8</sup>Brown, R. G. and Hwang, P. Y., *Introduction to Random Signals and Applied Kalman Filtering*, John Wiley and Sons, Inc., New York, NY, 3rd ed., 1997.

<sup>9</sup>Hermann, R. and Krener, A. K., "Nonlinear Controllability and Observability," *IEEE Transactions on Automatic Control*, Vol. AC-22, No. 5, Oct. 1977, pp. 728–740.

<sup>10</sup>Gauthier, J. P., Hammouru, H., and Othman, S., "A Simple Observer for Nonlinear Systems, Application to Bioreactors," *IEEE Transactions on Automatic Control*, Vol. AC-37, No. 6, June 1992, pp. 875–880.